Nonlinear Dynamics **xxx:** 1–16, 2004.

Identifying Multidimensional Damage in a Hierarchical Dynamical System

DAVID CHELIDZE
Department of Mechanical Engineering and Applied Mechanics, University of Rhode Island, Kingston, RI 02881, USA;
E-mail: chelidze@egr.uri.edu

(Received: 11 August 2003; accepted: 28 June 2004)

Abstract. In this paper, we present a novel method for multidimensional damage identification based on a dynamical systems approach to damage evolution. This approach does not depend on the knowledge of particular damage physics, and is appropriate for systems where damage evolves on much slower time scale than the directly observable dynamics. In an experimental context, the phase space reconstruction and locally linear models are used to quantify small distortions occurring in a dynamical system's phase space due to damage accumulation. These measurements are then related to the drifts in damage variables. A mathematical model of a harmonically driven cantilever beam in a force field of two battery-powered electromagnets is used to demonstrate validity of the method. It is explicitly demonstrated that an affine projection of the described feature vector accurately tracks the two competing damage processes. For practical damage identification purposes, the tracking data is analyzed using the proper orthogonal decomposition (POD) and smooth orthogonal decomposition (SOD) methods. Both methods correctly identify the two dominant damage modes. However, the SOD is more impervious to changes in fast-time dynamics and provides a significantly better signal-to-noise ratio. The damage modes identified using SOD are demonstrated to be within a linear transformation from the actual damage states and can be used to reconstruct the corresponding phase space trajectory.

Key words: condition monitoring, diagnostics, dynamical systems, health monitoring, multidimensional damage identification, phase space reconstruction

1. Introduction

The development of machinery and structural health monitoring technology is one of the important tasks of current applied engineering research. This is a formidable undertaking, considering the complex and hidden nature of damage. Damage can refer to any variety of physical processes that cause degradation in a system's performance leading to imminent failures. Existing literature abounds with solutions to some particular *imminent damage* detection problems (e.g., material fracture, sensor or power source failure, etc.) that mainly focus on scalar damage processes. Current research efforts, however, move past such alarm-based diagnostics of scalar variables to *gray scale* health monitoring of *incipient* multi-valued damage processes, which is required for the development of true prognostic ability.

Most of the early mechanical systems damage identification work focused on damage detection [1]. Data-based, or heuristic, approach is to look for changes due to the damage accumulation in time or frequency domain statistics [2], or in statistics that have both time and frequency information [3]. For nonlinear systems exhibiting chaotic response it is customary to use estimates of long-time chaotic invariant measures, such as the correlation dimension [4]. Other advanced techniques use expert systems or fuzzy logic [5]. The main advantages of such methods are simplicity of implementation and that they often work very well. Most heuristic methods serve as purely damage detection methods; i.e., no damage state assessment is provided. Even when the severity of damage can be estimated [6], it is usually very

hard to establish a direct one-to-one connection between the damage state and the change in the heuristic statistic or feature vector. There is no theoretical basis for predicting a priori, without the benefit of a good model or experiment, whether a certain feature vector will work well for a particular system.

A model-based approach addresses some of the shortcomings of the purely statistical approach at the expense of a more difficult development and implementation [7]. In rare cases, when the system's analytical model is available, it is usually possible to establish a functional connection between the drifting model parameters and a particular feature vector [8]. The lack of analytical models is customarily addressed by developing finite elements or data-based models. For linear systems, for example, autoregressive model parameter spectra and linear prediction error are used for fault detection in ball bearings [9] and gears [10], respectively. As another example, the frequency response functions are widely used for damage detection [11] in structures. Nonlinear systems are usually modeled using neural networks [12] for the same purpose. Other successful approaches are based on some type of hybrid method. For example, extensive attention is allotted to the use of mode shapes, or their curvatures, for damage detection and identification [13]. However, in many cases these methods are application dependent, and the main advantage of a model-based approach, which is to correlate the changes in a feature vector with the changes in a system's physical parameters, is lost.

In this paper, a multidimensional damage diagnosis method is developed. It is based on a dynamical systems approach to damage evolution [14]. Damage diagnosis is accomplished using a concept of phase space warping [15–17], which refers to small distortions in the phase space of a system due to the damage accumulation. In [18] the application of the earlier version of the method to identifying and tracking a scalar material damage process is demonstrated. The method presented here is able to track competing damage modes that evolve on slower time scales than the directly observable dynamics of a system. For systems undergoing abrupt or catastrophic changes the method is not able to provide tracking. However, it can still detect and quantify these changes.

In the next section, a brief description of the dynamical systems approach to damage evolution is given. A new multidimensional damage tracking metric is introduced next, and a novel strategy for damage identification is described. Application of the proposed techniques to a model of an electromechanical system with drifting potential field is described next. The results of two-dimensional damage identification and their implications are discussed at the end, followed by conclusions.

2. Dynamical Systems Approach to Damage Evolution

In this section, a brief summary of main ideas fully described in [15, 17] is given for completeness. In the dynamical systems approach [14], damage is viewed as a point evolving in an extended phase space of a hierarchical dynamical system. In this system, slow-time damage evolution causes parameter drifts in a subsystem describing dynamics of directly observable fast-time variables:

$$\dot{\mathbf{x}} = \mathbf{f}(\mathbf{x}, \boldsymbol{\mu}(\boldsymbol{\phi})), \tag{1a}$$

$$\dot{\boldsymbol{\phi}} = \epsilon\, \mathbf{g}(\boldsymbol{\phi}, \mathbf{x}), \tag{1b}$$

where $\mathbf{x} \in \mathbb{R}^n$ is a directly observable, fast-time variable; $\boldsymbol{\phi} \in \mathbb{R}^m$ is a hidden damage, slow-time variable; $\boldsymbol{\mu} \in \mathbb{R}^s$ is a function of $\boldsymbol{\phi}$ representing the parameters in Equation (1a); a rate constant $0 < \epsilon \ll 1$ defines a time-scale separation between fast- and slow-time dynamics; and overdots denote differentiation with respect to time t. Over the time scales of $\mathcal{O}(\epsilon)$ we consider Equation (1a) to be quasistationary, since drifts in $\boldsymbol{\mu}$ are negligible.

This formulation is appropriate for systems where damage accumulation can be characterized by a time scale that is several orders of magnitude larger than a time scale associated with dynamic response of a corresponding structure. The methods presented here do not need the particular knowledge of Equation (1). However, they implicitly assume the existence of such a deterministic model. In the following, we develop main ideas behind multidimensional damage tracking strategy.

2.1. The Phase Space Warping Tracking Function

In an experimental context, the analytical form of governing differential Equations (1) is usually not available. However, measurements from the fast-time system (1a) that are in some functional relationship with the fast-time variable $\mathbf{x}$ are available. For practical purposes, these measurements are assumed to be a scalar smooth function of fast-time dynamics that couples all active degrees-of-freedom. Measured time series are usually sampled at uniform time intervals t_s, and the dynamics (i.e., the equivalent topological structure of the extended phase space) of Equation (1a) can be reconstructed using a delay coordinate embedding [19]. In this procedure, the measured scalar time series $\{x(r)\}_{r=1}^{M}$ is converted to a series of vectors $\mathbf{y}^T(r) = [x(r), x(r+\tau), \ldots, x(r+(d-1)\tau)] \in \mathbb{R}^d$, where τ is a suitable delay, and d is the appropriate embedding dimension. Embedding parameters, τ and d, are usually determined using the first minimum of the average mutual information [20] and method of false nearest neighbors [21], respectively.

The reconstructed state vectors are governed by an as yet unknown map of the form

$$\mathbf{y}(r+k) = \mathbf{P}_k(\mathbf{y}(r); \boldsymbol{\phi}), \tag{2}$$

where $\mathbf{P}_k : \mathbb{R}^d \to \mathbb{R}^d$ is generally nonlinear. The drift in the damage variable $\boldsymbol{\phi}$ will cause distortions in the phase space, altering the evolution of trajectories. The *phase space warping* (PSW) refers to these changes in the vector field. In previous work [15, 16], the following *PSW tracking function*

$$\mathcal{E}_k(\mathbf{y}; \boldsymbol{\phi}) = \mathbf{P}_k(\mathbf{y}; \boldsymbol{\phi}) - \mathbf{P}_k\left(\mathbf{y}; \boldsymbol{\phi}_0\right) \tag{3}$$

was proposed for damage identification. In Equation (3) $\boldsymbol{\phi}_0$ is the reference or healthy state of the damage variable.

Note that, for a fixed point $\mathbf{y}$, the PSW tracking function can be expanded into a Taylor series in $\boldsymbol{\phi}$ about the reference value $\boldsymbol{\phi}_0$. For $\boldsymbol{\phi}$ sufficiently close to $\boldsymbol{\phi}_0$, it is shown in [15] that, assuming *linear observability* (i.e., the first derivative of $\mathbf{P}_k$ with respect to $\boldsymbol{\phi}$ has maximal rank), the relationship between the PSW tracking function and the damage variable can be well-approximated by an affine map $\mathcal{C} : \mathbb{R}^m \to \mathbb{R}^d$

$$\mathcal{E}_k(\mathbf{y}; \boldsymbol{\phi}) = \mathbf{C}(\mathbf{y})\,\boldsymbol{\phi} + \mathbf{c}(\mathbf{y}) + \mathcal{O}(\|\boldsymbol{\phi} - \boldsymbol{\phi}_0\|^2), \tag{4}$$

where the matrix $\mathbf{C} = \partial \mathbf{P}_k / \partial \boldsymbol{\phi}$ is evaluated at $\boldsymbol{\phi} = \boldsymbol{\phi}_0$, and $\mathbf{c} = -\mathbf{C}\boldsymbol{\phi}_0$ is a column vector. Thus, under the above assumptions, the tracking function at any generic fixed point $\mathbf{y}$ can be used to provide a linear measurement of, and therefore a means of tracking, the damage variable $\boldsymbol{\phi}$.

To actually calculate the PSW tracking function $\mathcal{E}_k(\mathbf{y}; \boldsymbol{\phi})$ for any given point $\mathbf{y}$, we need to know how the fast subsystem evolves from this point over the time interval $k\,t_s$ for the current value of $\boldsymbol{\phi}$, as well as how this subsystem *would have* evolved for the reference value of $\boldsymbol{\phi}_0$. Since the system's fast-time behavior for the current value of $\boldsymbol{\phi}$ is directly measurable (i.e., we can reconstruct the fast-time

trajectory using a sensor measurement from the fast subsystem), the strategy is to compare it to the predictions of a *reference model* describing the fast subsystem's behavior for $\phi = \phi_0 + \mathcal{O}(\epsilon)$. Here, as in previous work, the local linear models are used as the simplest form of a globally nonlinear reference model

$$\mathbf{y}(r+k) = \mathbf{A}_k \mathbf{y}(r) + \mathbf{a}_k, \tag{5}$$

where $\mathbf{A}_k$ is an $d \times d$ matrix and $\mathbf{a}_k$ is an $d \times 1$ vector. Equation (5) approximates Equation (2) for a particular point $\mathbf{y}(r)$ in the reference system's reconstructed phase space. Note that in practical applications other modeling solutions, such as neural nets or auto regressive moving averages, may be more appropriate. The parameters of local linear models are determined by calculating the best linear fit between N nearest neighbors of $\mathbf{y}(r)$ and their future states $k\,t_s$ time later. Then the PSW tracking function (Equation (3)) for the point $\mathbf{y}(r)$ can be written as

$$\begin{aligned} \mathcal{E}_k(\mathbf{y}(r);\phi) &= \mathbf{y}(r+k) - \mathbf{A}_k\mathbf{y}(r) - \mathbf{a}_k + \mathbf{E}_k^M \\ &= \mathbf{E}_k(\mathbf{y}(r);\phi) + \mathbf{E}_k^M, \end{aligned} \tag{6}$$

where $\mathbf{E}_k^M$ represents the local linear model error, and

$$\mathbf{E}_k(\mathbf{y}(r);\phi) = \mathbf{y}(r+k) - \mathbf{A}_k\mathbf{y}(r) - \mathbf{a}_k \tag{7}$$

is the *estimated tracking function* that can be determined experimentally for any point $\mathbf{y}(r)$ on the reconstructed trajectory. The use of $\mathbf{E}_k$ in place of $\mathcal{E}_k$ is justified if $\mathbf{E}_k^M$ is small compared to $\mathbf{E}_k$.

3. Multidimensional Damage Diagnosis

Hypothetically, if the system Equation (1) is started from the same initial condition $\mathbf{y}$ for different values of damage variable ϕ, then the estimated tracking function Equation (7) is expected to linearly track the damage variable, assuming there is negligible modeling error and linear observability conditions are satisfied. In practice, one cannot start the system from the same initial condition and has to infer the damage condition from the available dynamic measurements.

Using the procedure described in previous section, the estimated tracking metric can be calculated for every point on trajectories reconstructed from each data record. In previous work [15–17], a tracking metric based on a suitable average of the tracking function over all points on the trajectory, $\langle \|\mathbf{E}_k(\mathbf{y};\phi)\| \rangle_{\mathbf{y}}$, was successfully used to track a scalar battery voltage variable and to identify a scalar material damage process. However, as discussed in detail in [17], in general there will be fluctuations in the tracking metric caused by two main sources not related to changes in damage variable ϕ.

The first source of the superfluous fluctuations is the change in the population of points from data record to data record. These changes are caused by the drifts in parameters of fast subsystem Equation (1a) effected by slow damage evolution. This process is prone to trigger changes (or bifurcations) in the quasi steady state behavior of the fast subsystem due to structural instability. In fact, in our previous experimental work, repeated transitions from chaotic to periodic motions were observed throughout the experiments.

The second source of the extraneous variability in the estimated tracking metric is attributed to the changes in the actual mapping of Equation (2) from point to point in the phase space. In addition, because

of uneven distribution of points in the reconstructed reference phase space, we will have variability in the model fit error $\mathbf{E}_k^M$, also from point to point. The factors causing these variabilities are stemming from the nonlinearities in Equations (1a) and (2). However, for a linear model of fast-time dynamics these fluctuations are expected to be considerably reduced.

In [15, 16], all extra fluctuations were reduced by an appropriate probability density weighted average, and a recursive filtering was used for the same purpose in [17]. In what follows we describe a new multidimensional damage feature vector that is also aimed at reducing the spurious variability described here.

3.1. Multidimensional Damage Feature Vector

Ideally, we want to compare the estimated damage tracking functions for the same fixed points in the reconstructed phase space. In practical experimental context, we can only estimate the tracking function for every point on the trajectory reconstructed from the recorded data. Unfortunately, each data record will have different trajectory and, therefore, different population of points. Alternatively, we may try to compare the expected values of the tracking function in some local neighborhoods of the reconstructed phase space. Therefore, our new approach is to evaluate the expected value of the estimated tracking function $\mathbf{E}_k(\mathbf{y}; \phi)$ in N_e disjoint regions $\mathcal{B}_i$ ($i = 1, \ldots, N_e$) of the reconstructed phase space

$$\mathbf{e}_k^i(\phi) = \|\mathcal{B}_i\|^{-1} \sum_{\mathbf{y} \in \mathcal{B}_i} \mathbf{E}_k(\mathbf{y}; \phi), \tag{8}$$

and combine them in one *multidimensional damage feature vector*:

$$\mathbf{S}_k(\phi) = \left[\mathbf{e}_k^1; \mathbf{e}_k^2; \ldots; \mathbf{e}_k^{N_e}\right], \tag{9}$$

where each data record will have a total of $N_s = d \times N_e$ ($\mathbf{S}_k \in \mathbb{R}^{N_s}$) statistics.

In addition to the ability to track multidimensional damage variables, this feature vector has an added benefit of compensating for the spurious fluctuation observed in previous tracking metrics. We generally expect the system to go through the bifurcations in its steady state behavior as parameters drift due to damage. However, when using the new feature vector there is a higher probability that at least some of the local neighborhoods $\mathcal{B}_i$ will have sufficiently similar populations of points to yield meaningful components of $\mathbf{S}_k$ throughout of the experiment. The other sources of fluctuations in the tracking unrelated to damage are also reduced by the new feature vector. Since each $\mathbf{e}_k^i$ is evaluated in local neighborhood, the variability in the the mapping Equation (2) and modeling error are minimized.

The choice of parameter k effects the choice of appropriate local neighborhoods as discussed in [18]. The data sampling rate and the signal-to-noise ratio of acquired data will dictate the minimum acceptable value for k—it needs to be large enough to differentiate between the variabilities due to noise and damage. For nonlinear systems with chaotic response, the sensitive dependence on initial conditions imposes a prediction horizon and, therefore, upper limit on k. To reduce the fluctuations due to the variability in the mapping Equation (2), we need to choose local neighborhoods so that Equation (2) has approximately uniform sensitivity to damage within each neighborhood. The choice of neighborhoods for large values of k can be complicated [18]: as k increases the large sensitivities clusters near unstable manifold, which can be a fractal object. However, for small values of k the

sensitivities are arranged in the linear fashion in phase space, which makes sectioning of phase space into the regions of uniform sensitivity easier.

Based on the above and Equation (4), it is conjectured that there is an affine projection $\mathcal{V} : \mathbb{R}^{N_s} \to \mathbb{R}^m$ that maps the proposed feature vector onto the damage state:

$$\phi = \mathbf{V}\mathbf{S}_k + \mathbf{v}, \tag{10}$$

where $\mathbf{V}$ is an $m \times N_s$ matrix, and $\mathbf{v}$ is an $m \times 1$ vector.

Affine projection parameters, $\mathbf{V}$ and $\mathbf{v}$, can be determined if independent measurements of damage state are available. In an experiment, a total of N_r data records are collected and an $(N_s + 1) \times N_r$ matrix $\mathbf{W}$ is formed, such that $\mathbf{W}^i = [(\mathbf{S}_k^i); 1]$ for each data record $i = 1, \ldots, N_r$. Then, an $m \times N_r$ matrix $\mathbf{\Phi}$ is formed, where $\mathbf{\Phi}_i = \langle\phi\rangle_i$ is composed of the average values of ϕ for each data record i. Thus, the needed affine transformation can be calculated in the least-squares sense:

$$[\mathbf{V}, \mathbf{v}] = \mathbf{\Phi}\mathbf{W}^T(\mathbf{W}\mathbf{W}^T)^{-1}. \tag{11}$$

The direct measurement of damage state or means to estimate the affine projection parameters of Equation (11) are not present in many practical situations. Therefore, the feature vector has to be used directly to determine the observable facts about the hidden damage state. For this purpose, $\mathbf{S}_k$ is estimated for each of N_r data records. They are arranged in a $N_r \times N_s$ *tracking matrix* $\mathbf{Y}$. Each column of this matrix is normalized by subtracting its mean, and scaling it to unit norm. Here, two different approaches to this problem are explored. The first is based on the *proper orthogonal decomposition* (POD) [22] of the tracking matrix, and the second on the *smooth orthogonal decomposition* (SOD) (or optimal tracking [25]).

3.2. POD-Based Damage Identification

The POD or Karhunen-Loève decomposition is often used to identify active states in a nonlinear dynamical system and develop reduced order models [22, 23]. Proper orthogonal modes (POMs) have also been instrumental in studying linear and nonlinear mode interactions in systems [24]. Using the discrete version of the POD or *singular value decomposition* (SVD) the matrix $\mathbf{Y}$ can be written in the form

$$\mathbf{Y} = \mathbf{U}\mathbf{\Lambda}\mathbf{V}^T, \tag{12}$$

where $\mathbf{U}$ $(N_r \times N_r)$ and $\mathbf{V}$ $(N_s \times N_s)$ are unitary matrices, and $\mathbf{\Lambda}$ is a diagonal matrix of size $N_r \times N_s$ containing N_s singular values, which are arranged in decreasing order. The first i columns of matrix $\mathbf{V}$, corresponding to the largest i singular values, give an optimal orthonormal basis for approximating the data in i-dimensions. Magnitude of a singular value corresponds to the amount of "energy" in the projection of matrix $\mathbf{Y}$ span by a corresponding column of $\mathbf{V}$. The *POD-based tracking metric*, φ_p, will be given by the columns of $\mathbf{U}$ or the POMs corresponding to the largest singular values of $\mathbf{Y}$.

It is hypothesized that the POD analysis will reveal the number of active damage states in the experiment. In other words, for m active damage modes only m dominant POMs will be identified, and these POMs will be within a linear transformation of actual damage modes.

3.3. SOD-Based Damage Identification

The SOD is based on the optimal tracking method that was first proposed for scalar damage processes identification in [25]. This method relies on the existence of underlying deterministic behavior of the damage accumulation process, but does not require its model. It assumes that the damage accumulation process follows some smooth trend. Thus, *smooth orthogonal mode* (SOM) is found by maximizing smoothness and overall variation in a projection of the tracking matrix, found by solving a generalized eigenvalue problem.

The SOD can be viewed as a constrained version of POD, where an additional constraint is introduced requiring the POMs to be smooth. Given the matrix $\mathbf{Y}$, we are looking for its linear projection $\varphi_s = \mathbf{Y}\mathbf{q}$ that varies smoothly and has a maximum variation. This problem reduces to the following constrained maximization problem:

$$\max_{\mathbf{q}} \|\varphi_s\|^2 \quad \text{subject to} \quad \|\mathbf{D}\varphi_s\|^2 = 1, \tag{13}$$

where $\mathbf{D}$ is a $(N_r - 1) \times N_r$ differential operator

$$\mathbf{D} := \begin{bmatrix} 1 & -1 & 0 & \dots & 0 \\ 0 & 1 & -1 & \dots & 0 \\ \vdots & \ddots & \ddots & \ddots & \vdots \\ 0 & \dots & 0 & 1 & -1 \end{bmatrix}. \tag{14}$$

Using Euler-Lagrange equation, one can easily show that Equation (13) is equivalent to the following generalized eigenvalue problem:

$$\left[\mathbf{Y}^T\mathbf{Y}\right]\mathbf{q} = \lambda\left[(\mathbf{D}\mathbf{Y})^T\mathbf{D}\mathbf{Y}\right]\mathbf{q}. \tag{15}$$

The eigenvector $\mathbf{q}$ corresponding to the largest eigenvalue λ of Equation (15) yields the optimal projection of matrix $\mathbf{Y}$ that maximize the smoothness and the overall variation of damage observer φ_s. For practical purposes, as with the POD, the solution to Equation (15) is obtained using *generalized singular value decomposition* (GSVD) of $[\mathbf{Y}^T\mathbf{Y}, (\mathbf{D}\mathbf{Y})^T\mathbf{D}\mathbf{Y}]$ matrices [26].

It is hypothesized that in the presence of m-dimensional damage evolution the above procedure will yield m generalized eigenvalues of Equation (15) that will be several magnitudes of order larger than the rest; and the corresponding *SOD-based tracking metric* φ_s will be within a linear transformation of the actual damage state variable ϕ.

4. Model of an Electromechanical System

A numerical experiment is conducted using a model of an experimental apparatus, described in [15, 16]. This system is a constrained version of a vibrating clamped-free beam in the force field of two permanent magnets [27]. The only difference with the previous system was that one permanent magnet was augmented by an electromagnet. In this paper, *both* permanent magnets are outfitted with identical electromagnets. The force field at the beam tip drifts as the batteries powering the electromagnets discharge. The model parameters are chosen so that a complete discharge of the batteries manifests

itself in about a 3.5% change in the natural frequencies of small oscillations in each electromagnet's well.

As in [16] the system can be viewed as a mechanical subsystem coupled with an electromagnetic subsystem. The derivation of the mathematical model is identical to one presented in [16], with the exception of one additional electromagnet circuit. Therefore, without going into details, we present a final dimensionless form of the equations of motion for a single mode of the beam vibration

$$\ddot{\theta} + \mu\,\dot{\theta} + (1-\alpha_1)\,\theta + \alpha_3\,\theta^3 + \sum_{i=1}^{2} \frac{\kappa L_r\,(\theta-\lambda_i)}{\left(1+\kappa\,(\theta-\lambda_i)^2\right)^2}\,\psi_i^2 = f\,\cos\Omega t. \tag{16}$$

This equation is coupled to a set of equations (for $i = 1, 2$) describing the current flow in the electromagnets' circuits:

$$\left[1 + \frac{L_r}{1+\kappa\,(\theta-\lambda_i)^2}\right]\dot{\psi}_i + \left[r - \frac{2\,\kappa\,L_r\,(\theta-\lambda_i)\,\dot{\theta}}{[1+\kappa\,(\theta-\lambda_i)^2]^2}\right]\psi_i = \phi_i\,. \tag{17}$$

In Equations (16)–(17) θ, ψ_1 and ψ_2 represent fast-time dynamic variables describing beam displacement and electrical current oscillations; μ accounts for mechanical viscous damping; α_1 and α_3 describe the shape of the potential field; κ indicates the strength of the coupling between the mechanical and electrical oscillations; L_r describes the electromagnets' inductance; $\lambda_1 = -\lambda_2$ indicate the position of the electromagnets; f is a forcing amplitude; Ω is a ratio of forcing and natural frequencies; r describes the total resistance of the circuits; and ϕ_1 and ϕ_2 represent slow-time damage variables or the dimensionless battery voltages.

The time evolution of the battery voltage is governed by electrochemical processes, which are not explicitly modeled. Instead, given the experimental battery voltage evolution trends typically seen in the experiments[15], the following voltage evolution law for both batteries is used,

$$\dot{\phi}_i = -\epsilon_i\,(\phi_i - \xi)(1+\gamma(\phi_i-\eta)^2)\;(i=1,2), \tag{18}$$

where ξ, γ and η are positive constants, and the rate constant ϵ_i satisfies $0 < \epsilon_i \ll 1$.

Equations (16)–(18) were integrated numerically with a standard forth-order variable-step-size Runge-Kutta algorithm. Since this study was inspired by the experimental investigation of a scalar damage tracking method, the parameters for the model were selected to match the properties of the experimental system in key ways, as described below.

It is assumed that fully charged batteries provide 9 V DC power. It is also assumed that the natural frequency of small oscillations in the potential well with the electromagnet changes by 3.5% from 8.8 to 8.5 Hz. The effective mass, $m = 0.2$ kg, and length, $l = 0.128$ m, were obtained directly from the experiment. A fourth-order polynomial fit to a histogram of the experimental reference data was used to estimate $\alpha_1 = 2.6558$ and $\alpha_3 = 0.8805$. The effective damping parameter was assumed to be $\mu = 0.088$.

By linearizing Equations (16), and (17) about the stable equilibria ($\theta = \pm\sqrt{(\alpha_1-1)/\alpha_3}$) for zero battery voltages, expressions for the frequency of small oscillations were obtained, which were used to estimate the effective stiffness k. Since the frequency for zero battery voltage in both electromagnets' wells is 8.5 Hz, one can estimate $k = 0.071$ using m, l, and α_1. We chose $\kappa = 0.746$, so that the effect of L_r on inductance amplitude decreased to 10% at 2λ distance. To determine other parameters, the case of one fully charged ($\Phi_1 = 9$V) and the other fully discharged ($\Phi_2 = 0$V) batteries was

considered, for which the natural frequency in the powered electromagnet's well is 8.8 Hz. Using this information, we found $L_r = 0.079$ after arbitrarily setting $r = 10$. Forcing amplitude $f = 1$ and forcing frequency $\Omega = 1.95$ were chosen so that the system exhibited nominally chaotic motion throughout the experiment.[1]

Other parameters used in the simulations were $\eta = 22$, $\gamma = 1$ and $\xi = 0.1$. The rate parameters for battery evolution laws were chosen to be $\epsilon_1 = 1 \times 10^{-6}$ and $\epsilon_2 = 0.5 \times 10^{-6}$, so that the first battery discharged twice as fast as the second. Using the above parameters, the dimensionless battery voltage $\phi = 2.846\,\mathbf{\Phi}$, and the observed fast-time dynamics of the simulated θ were found to have qualitatively similar trajectories in the $(\theta, \dot{\theta})$ phase space to those observed with experimental strain-gauge time series.

5. Results of Damage Identification

The total of 3×10^6 data points for each state variable were collected with a dimensionless sampling time of $t_s = 0.1$ during the numerical integration of Equations (16–18). The initial condition used in this simulation was obtained after integrating stationary fast-time equations for 200 forcing cycles to allow transients to die off. At the end of the simulation, both ϕ_1 and ϕ_2 variables reached a ξ value. For damage identification purposes, only the beam angular deflection θ time series was used. The first 2^{14} data points of the scalar θ data set were used for the reference model. Average mutual information and false nearest neighbors algorithms were used to select a delay of $\tau = 7$ sample steps, and an embedding dimension of $d = 6$ for the reference data set. The average pointwise dimension of the reference data set was approximately 2.7, supporting our assumption of a nominally chaotic system.

For the feature vector calculation, Equation (10), the entire data set was divided into consecutive data records of 2^{12} reconstructed points each (i.e., $M = 2^{12}$ and $N_r = 732$), and the sixteen nearest neighbors were used for the reference model construction. Since our data was practically noise free, there was no lower limit on the value of parameter k. However, since our reference system exhibited nominally chaotic behavior, appropriate sectioning of phase space was complicated for large values of k. Therefore, we set $k = 1$ and partitioned the reconstructed reference phase space into sixteen disjoint slabs uniformly distributed along the third coordinate of the reconstructed state vectors. The middle coordinate was used to circumvent any edge effects present in the reconstruction.

The feature vector $\mathbf{S}_1$ was determined by evaluating the tracking function in each of the phase space partitions or slabs. Thus, the 732×96 tracking matrix $\mathbf{Y}$ was formed. This matrix $\mathbf{Y}$ was normalized by subtracting the mean from each row and scaling it to the unit norm. Some of the rows of matrix $\mathbf{Y}$ contained discernable trends corresponding to battery discharge curves (see Figure 1). However, large local fluctuations in all the rows of the matrix were also present. These are the result of changes in the population of points from one data record to another. By itself, this change is the result of our system going through bifurcations as hidden slow parameters drift.

In this numerical study, all the slow-time damage variables are available. Therefore, the affine transformation of Equation (10) can be estimated using Equation (11). Results of this calculation are plotted in Figure 2. The graphs in the left column of this figure show the estimated (gray dots) and actual (black line) battery voltages versus time; in the right column the calibration curves are shown, where estimated battery voltages are plotted versus corresponding true battery voltages. The black line in the calibration

[1]No tests for chaos were performed for these numerical experiments, since the existence or nonexistence of chaos is not particularly relevant to the task at hand.

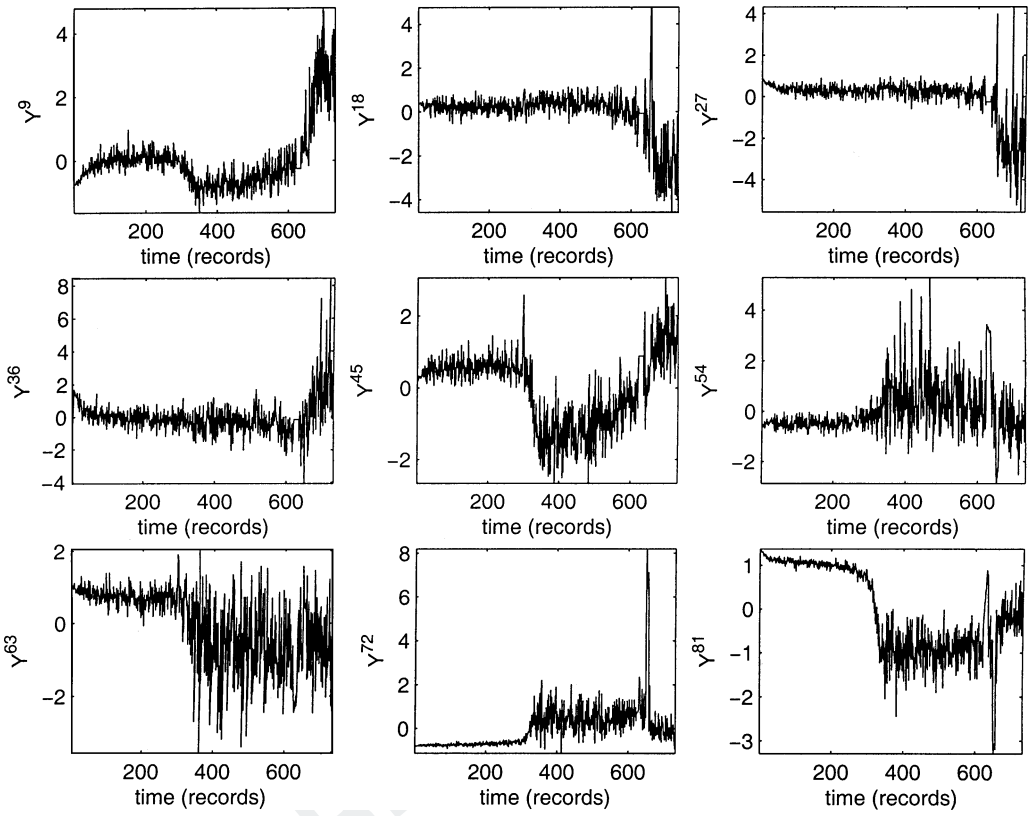

Figure 1. Sample of some of the rows of the estimated tracking metric **Y**.

figures shows the corresponding linear fit to the data. Any deviation from the linearity during the large drop in the voltages can be explained by the effect of higher order terms in Equation (10). The accuracy of these estimates can be further improved by accounting for the precision of the local linear model within each slab when calculating $\mathbf{S}_1$, Equation (9), as shown in [15]. However, this is left for future development.

In many practical situations, the direct measurement of a damage state is not available, and one is forced to infer the facts about the hidden damage state from the available statistics. Therefore, for damage identification purposes, the tracking data was analyzed using the POD- and SOD-based damage identification procedures. In this analysis it is not expected to find the exact curves shown in Figure 2. These curves are just particular projections of the damage accumulation trajectory from the three-dimensional extended phase space of the battery voltage $(\phi_1, \phi_2, t) \in \mathbb{R}^3$ onto the planes parallel to time axis. However, as hypothesized, it is expected to find other equivalent projections of this curve that are linear transformations of the original. In other words, the trajectory in the battery voltage phase space should be topologically equivalent to the original.

The results of the POD-based identification are shown in Figure 3(a), (b), and (c). Figure 3(a) shows the first twenty singular values of matrix **Y**. In this figure, first two singular values are clearly separated from the rest; however, they are not significantly larger than the rest. In Figure 3(b) and (c) the corresponding first two POMs are shown. The amount of local fluctuation in these modes is considerably smaller compared to the graphs in Figure 1. However, the existence of a large periodic window in data records 625–635 produces a noticeable kink in the trend that is not attributed to the damage evolution.

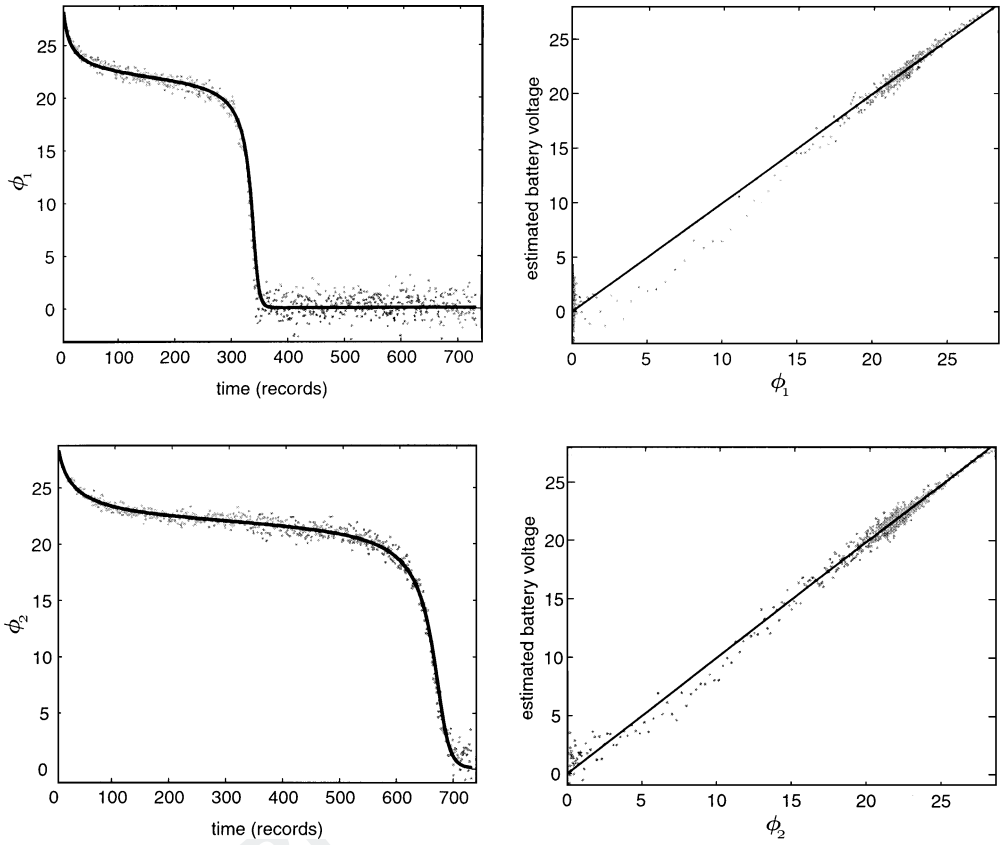

Figure 2. Left column: Affine projections of the damage tracking matrix (gray dots) and actual battery voltage (black lines) versus time. Right column: Corresponding calibration curves (gray dots) with least-squares linear fit (black lines).

The results of the SOD-based identification applied to the tracking matrix **Y** are shown in Figure 3(d), (e), and (f). The first twenty generalized eigenvalues of Equation (15), are depicted in Figure 3(d). Here, the first two generalized eigenvalues are clearly several orders of magnitude larger then the rest. The SOMs that correspond to these first two eigenvalues are shown in Figure 3(e) and (f), respectively. In these modes, the local fluctuations are greatly reduced compared to the POMs shown in Figure 3(b) and (c). In addition, these graphs do not suffer from the presence of large periodic windows in the data records and provide consistent trends that can be directly related to the damage evolution curves.

Both the POD- and SOD-based identification methods yield virtually identical trends. However, the underlying trend is more pronounced in the SOD calculation, which has significantly lower local fluctuations and does not suffer from changes unrelated to damage evolution. Therefore, in further analysis only these two SOMs are used.

Figure 4 shows the battery voltage phase portrait and the corresponding trajectory obtained using the identified SOMs. It is apparent that both trajectories have qualitatively similar trends in the phase portraits. The simulation starts with gradual decrease in the voltage of both batteries, identified in the phase portraits by a region (a). The region (a) is followed by a rapid decrease (failure) in the first battery voltage, marked by region (b). This is consecuently followed by a rapid decrease in the second battery voltage also, region (c). All the regions clearly visible in actual phase portrait are also present in the reconstructed trajectory obtained using SOD-based identification.

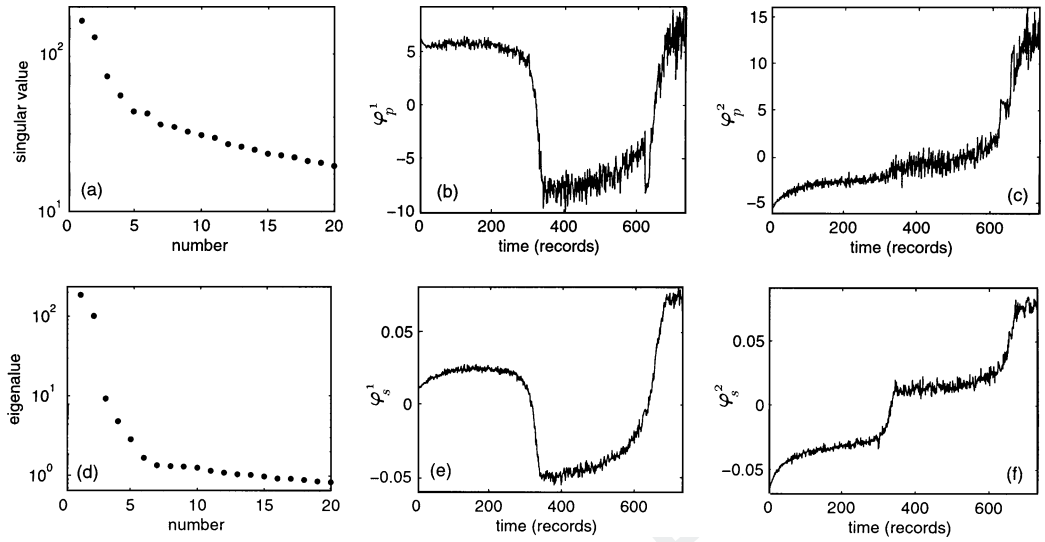

Figure 3. (a) First twenty singular values of damage tracking metric **Y**. (b) and (c) POMs corresponding to the first two singular values. (d) First twenty generalized eigenvalues of [**A**, **B**], 15. (e) and (f) SOMs corresponding to the first two generalized eigenvalues.

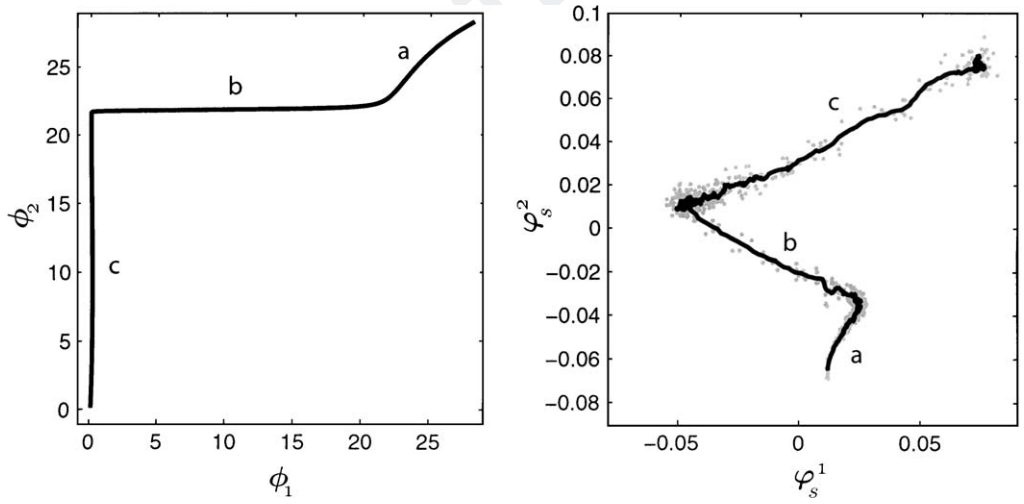

Figure 4. Actual phase portrait of battery voltage evolution (left plot) and identified phase portrait of SOMs (right plot). The light gray dots show actual SOMs, and the black line represents a moving average of this data over consecutive 10 points.

The hypothesis about existence of linear one-to-one correspondence between the actual battery voltages and the identified SOMs can be confirmed if there exists a linear transform mapping the SOMs onto the battery voltages. The affine transformation relating the first two SOMs to the actual damage variables was determined in the least-squares sense. The result of this calculation is shown in Figure 5. The graphs in the left column of this figure show the SOMs after the affine transformation and actual battery voltage plotted versus time; the right column shows the corresponding calibration curves, where the SOD-based tracking observers are plotted versus actual battery voltages. The black line in these figures shows the corresponding linear fit to the data.

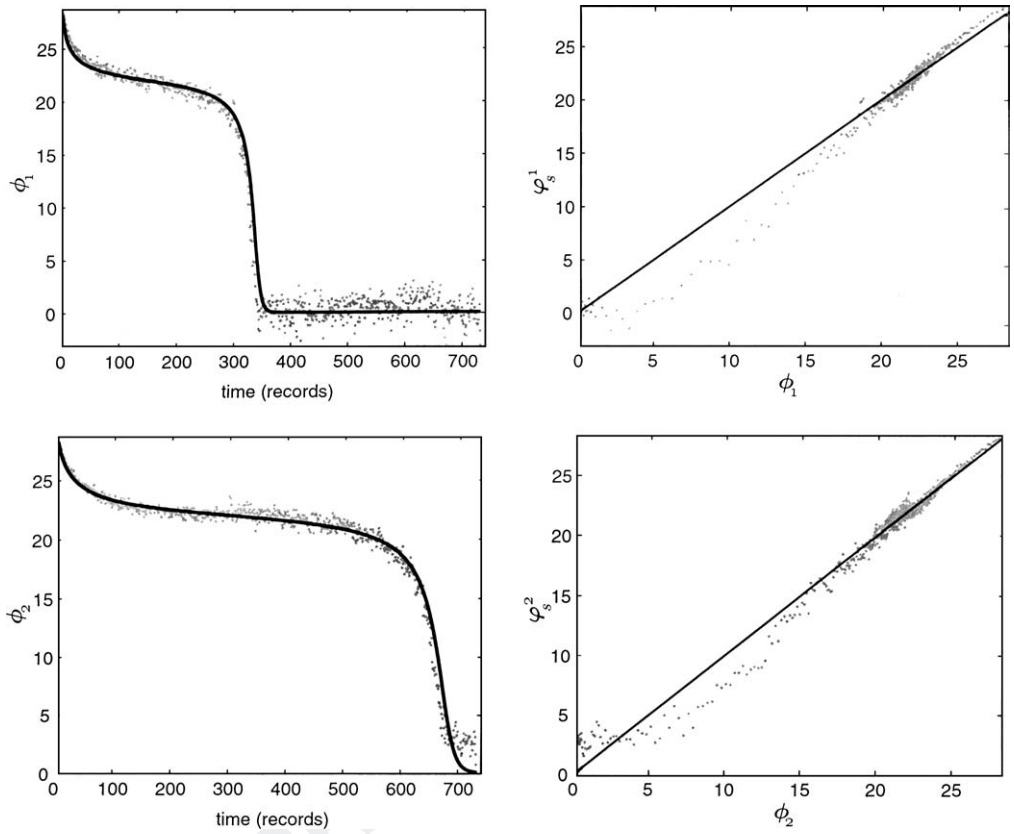

Figure 5. Left column: Scaled SOMs (gray dots) and actual battery voltage (black lines) versus time. Right column: Corresponding calibration curves (gray dots) with least-squares linear fit (black lines).

6. Discussion

The tracking results based on the simulated experiment show that the tracking algorithm accurately recovers (within an affine projection) the theoretical tracking curves for both simultaneously evolving slow damage variables, as shown in Figure 2. This confirms our conjecture that the feature vector $\mathbf{S}_k$ can be projected onto the damage state variable ϕ using Equation (10). The local fluctuations present in this tracking metric are the result of changes in the population of points from data record to data record and the inaccuracy of the local linear models. These results can be further improved by incorporating probability density function weighted averages as in [15], and using stochastic interrogation [27] to maximize uniformity of point populations within separate data records.

Another hypothesis is that the POD- and SOD-based analysis yield a proper number of active damage modes. The results conclusively confirmed that this is indeed true for the identified SOMs and, to a lesser extent, for the identified POMs. The generalized eigenvalues calculated in the SOD procedure clearly identify the two most dominant modes that satisfy the *optimality criteria*, which are maximization of smoothness and overall variation. However, the singular values obtained in POD analysis are not as clearly differentiating. However, it is apparent that a significant amount of energy related to damage accumulation is still present in the higher order POMs.

Our final hypothesis is that the identified POMs and SOMs are within an affine transformation of the actual damage states. Both the first two POMs and SOMs show strikingly similar trends. However, the SOMs have significantly smaller local fluctuations and do not suffer from the drastic change in fast-time system dynamics. When viewed in the battery voltage phase portrait (see Figure 4) the identified SOMs show topologically similar trajectory when compared to the actual battery voltage trajectory. The affine transformation of the SOMs provides an accurate tracking observer for the actual damage variables as shown in Figure 5.

These results clearly demonstrate that the POD-based damage identification is prone to be corrupted by the extraneous fluctuations caused by bifurcations in the fast-time dynamics. These bifurcations trigger abrupt changes in the steady state behavior of the fast-time system that filter down into the components of the feature vector Equation (9). However, the SOD-based identification scheme is immune to these sharp jumps in the metrics, since it is looking for the projections that evolve smoothly in time. Therefore, use of SOD is preferred for structurally unstable systems and only for structurally stable systems POD will yield equivalent results.

Figures 2 and 5 show another powerful result of this paper: the trends depicted in these figures match extremely well. Figure 2 was obtained by estimating an affine projection of the full tracking metric using the independently available measurements of damage. Figure 5, however, is depicting the results of an affine transformation of only first two SOMs obtained in the blind damage identification procedure. The small differences in the graphs are only noticeable for very large changes in the damage variables. Therefore, identified SOMs can provide accurate and consistent multidimensional damage observers, that can be used in experiments for verifying available damage evolution laws or developing empirical damage models.

Conclusions

In this paper, a novel multi-mode damage diagnosis method was presented. The multidimensional damage tracking feature vector was developed in the framework of a dynamical systems approach to damage evolution. This methodology does not depend on knowledge of particular damage physics. Instead, it provides experimental means to determine practically observable and observed facts of damage accumulation. The procedure implicitly uses the assumption that the system undergoing damage accumulation possesses time-scale separation, where damage accumulation occurs on a much slower time scale than the observable dynamics of a system.

A detailed description of the damage tracking algorithm was given. Experimental procedures for estimating tracking functions in a reconstructed phase space, calculation of the multidimensional feature vector, and appropriate damage observers were given before describing an application to a simulated experimental system. A mathematical model of a harmonically driven cantilever beam in a force field of two battery-powered electromagnets was used in the simulation. Terminal voltages of the discharging batteries were treated as the slow-time damage variables, and the angular deflection of the vibrating beam was considered to be the measurement of the fast-time dynamics. An empirical battery discharge model was used to describe the slow-time damage evolution.

The beam angular deflection data was used to reconstruct the phase space of the fast-time dynamics using a delay coordinate embedding. Initial fast-time data was used to build a data-based reference model predicting short-time evolution of trajectories in the reconstructed phase space. The PSW tracking metrics were evaluated in this reconstructed phase space by comparing the current fast-time trajectories to the predictions of the reference model. As the damage grew, the system underwent many

bifurcations causing repeated periodic/chaotic transitions. Nevertheless, the affine projection of the calculated damage tracking feature vectors was shown to accurately track the two-dimensional damage states corresponding to simultaneously discharging battery voltages.

The practical applicability of the method was validated by two different methods of damage identification. Both the SOD and POD methods provided similar trends. However, the SOD method was less susceptible to the effects of change in the directly observable dynamics and had a significantly better signal-to-noise ratio. It showed that only two SOMs satisfied the optimality criterion. These identified modes were shown to be within an approximately linear transform from the actual two-dimensional damage variable, which showed an extremely good match to the affine projections of the full tracking matrix. Therefore, SOD-based identification can be used in experiments to reconstruct a phase space trajectory of slowly evolving damage.

Acknowledgements

This work was supported by the NSF CAREER grant No. CMS-0237792 and University of Rhode Island Council for Research Grant.

References

1. Zou, Y., Tong, L., and Steven, G. P., 'Vibration-based model-dependent damage (delimination) identification and health monitoring for composite structures – a review', *J. Sound & Vib.* **230**(2), 2000, 357–378.
2. Worden, K., Manson, G., and Fieller, N. R. J., 'Damage detection using outlier analysis', *J. Sound & Vib.* **229**(3), 2000, 647–667.
3. Luo, G. Y., Osypiw, D., and Irle, M., 'Real-time condition monitoring by significant and natural frequencies analysis of vibration signal with wavelet filter and autocorrelation enhancement', *J. Sound & Vib.* **236**(3), 2000, 413–430.
4. Craig, C., Neilson, D., and Penman, J., 'The use of correlation dimension in condition monitoring of systems with clearance', *J. Sound & Vib.* **231**(1), 2000, 1–17.
5. Mechefske, C. K., 'Objective machinery fault diagnosis using fuzzy logic', *J. Sys. and Sig. Proc.* **12**(6), 1998, 855–862.
6. Swanson, D. C., Spencer, J. M., and Arzoumanian, S. H., 'Prognostic modelling of crack growth in a tensioned steel band', *Mech. Sys. & Sig. Proc.* **14**(5), 2000, 789–803.
7. Natke, H. G. and Campel, C., *Model-Aided Diagnosis of Mechanical systems: fundamentals, detection, localization, assesment*, Springer-Verlag, Berlin, 1997.
8. Loparo, K. A., Adams, M. L., and Lin, W., 'Fault detection and diagnosis of rotating machinery', *IEEE trans. Indust. Elect.* **47**(5), 2000, 1005–1014.
9. Dron, J., Rasolofondraibe, L., Couet, C., and Pavan, A., 'Fault detection and monitoring of a ball bearing benchtest and a production machine via autoregressive spectrum analysis', *J. Sound & Vib.* **218**(3), 1998, 501–525.
10. Wang, W. and Wong, A. K., 'Autoregresive model-based gear fault diagnosis', *J. Vib. & Acoustics* **124**(2), 2002, 172–179.
11. Sampaio, R. P. C., Maia, N. M. M., and Silva, J. M. M., 'Damage detection using the frequency-response-function curvature method', *J. Sound & Vib.* **226**(5), 1999, 1029–1024.
12. Worden, K., 'Structural fault detection using a novelty measure', *J. Sound & Vib.* **201**(1), 1997, 85–101.
13. Cornwell, P., Doebling, S. W., and, Farrar C. R., 'Application of the strain energy damage detection method to plate-like structures', *J. Sound & Vib.* **224**(2), 2000, 359–374.
14. Cusumano, J. P. and Chatterjee, A., 'Steps towards a qualitative dynamics of damage evolution', *Int. J Solids & Struct.* **37**(44), 2000, 6397–6417.
15. Chelidze, D., Cusumano, J. P., and Chatterjee, A., 'Dynamical systems approach to damage evolution tracking, part 1: Description and experimental application', *J. Vib. & Acoustics* **124**(2), 2002, 250–257.
16. Cusumano, J. P., Chelidze, D., and Chatterjee, A., 'Dynamical systems approach to damage evolution tracking, part 2: Model-based validation and physical interpretation', *J. Vib. & Acoustics* **124**(2), 2002, 258–264.
17. Chelidze, D. and Cusumano, J. P., 'A dynamical systems approach to failure prognosis', *J. Vib. & Acoustics* **126**(1), 2004, 1–7.
18. Chelidze, D. and Liu, M., 'Dynamical systems approach to fatigue damage identification', *J. Sound & Vib.*, in press.

19. Sauer, T., Yorke, J. A., and Casdagli, M., 'Embedology', *J. Stat. Phys.* **65**(3-4), 1991, 579–616.
20. Fraser, A. M. and Swinney, H. L., 'Independent coordinates for strange attractors from mutual information', *Phys. Rev. A* **33**(2), 1986, 1134–1140.
21. Kennel, M. B., Brown, R., and Abarbanel, H. D. I., 'Determining embedding dimension for phase-space reconstruction using a geometric construction', *Phys. Rev. A* **45**(6), 1992, 3403–3411.
22. Berkooz, G., Holmes, P., and Lumley, J. L., 'The proper orthogonal decomposition in the analysis of turbulent flows', *Annual Review of Fluid Mechanics* **25**, 1993, 539–575.
23. Cusumano, J. P., Sharkady, M. T., and Kimble, B., 'Experimental measurements of dimensionality and spatial coherence in the dynamics of a flexible-beam impact oscillator', *Philosophical Transactions of the Royal Society* **347**, 1994, 421–438.
24. Feeny, B. F. and Kappagantu, R., 'On the physical interpretation of proper orthogonal modes in vibrations', *J. Sound & Vib.* **211**(4), 1998, 607–616.
25. Chatterjee, A., Cusumano, J. P., and Chelidze, D., 'Optimal tracking of parameter drift in a chaotic system: Experiment and theory', *J. Sound & Vib.* **250**(5), 2002, 877–901.
26. Golub, G. H. and Van Loan, C. F., *Matrix Computations*, 3rd edn., Johns Hopkins Univ. Press, Baltimore, 1996.
27. Cusumano, J. P. and Kimble, B., 'A stochastic interrogation method for experimental measurements of global dynamics and basin evolution: application to a two-well oscillator', *Nonlinear Dynamics* **8**, 1995, 213–235.